Release of chlorine during oat straw pyrolysis doped with char and ammonium chloride

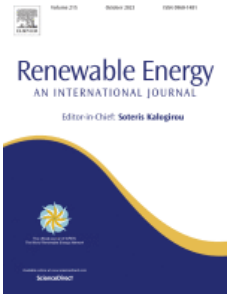

Wojciech Jerzak*, Mariusz Wądrzyk, Izabela Kalemba-Rec, Artur Bieniek, Aneta Magdziarz

DOI: https://doi.org/10.1016/j.renene.2023.118923

To appear in: *Renewable Energy*

Received Date: *6 January 2023*
Revised Date: *8 May 2023*
Accepted Date: *13 June 2023*

Please cite this article as: W. Jerzak, M. Wądrzyk, I. Kalemba-Rec, A. Bieniek, A. Magdziarz, Release of chlorine during oat straw pyrolysis doped with char and ammonium chloride, Renewable Energy (2023), doi: https://doi.org/10.1016/j.renene.2023.118923

Release of chlorine during oat straw pyrolysis doped with char and ammonium chloride

Wojciech Jerzak*, Mariusz Wądrzyk, Izabela Kalemba-Rec, Artur Bieniek, Aneta Magdziarz

AGH University of Krakow, Poland

e–mail*: wjerzak@agh.edu.pl

Keywords: Chlorine release, Biomass, Pyrolysis, Biochar

Abstract

Chlorine is one of the most undesirable elements in agricultural biomass which can cause operating problems during its thermal conversion. Even in low-temperature pyrolysis, chlorine is released in the gaseous phase. Therefore, in order to study the chlorine release during pyrolysis, the following samples were analyzed: oat straw, oat straw doped with char, oat straw doped with NH_4Cl, and char doped with NH_4Cl. The pyrolysis process of these feedstocks was conducted at 400, 500 and 600 °C under an inert atmosphere, with a short residence time (2 minutes) for a sample in the reactor. It transpired that the doping of ammonium chloride into oat straw increased the char yield. Doping oat straw with char as well as NH_4Cl promoted biochar carbonization. Chlorine release was significantly inhibited when increasing the pyrolysis temperature from 400 to 600 °C for samples of oat straw, oat straw doped with char, and oat straw doped with NH_4Cl. In addition, despite the increase in pyrolysis temperature, the percentage of chlorine distributed into the gas phase decreased. Doping oat straw with NH_4Cl had a positive effect on increasing the share of furfural (up to 12.9% at 400 °C) in non-condensed gases identified by pyrolysis gas chromatography-mass spectrometry.

1. Introduction

The average annual harvest of cereal straw in Poland has for many years exceeded the demand resulting from agricultural production. Although statistics show a downward trend in straw biomass surplus in recent years, 9.2 million tonnes of straw surplus is forecast in 2030 [1]. Therefore, it is legitimate to search for an effective way to manage waste straw. Straw biomass is an excellent alternative to solid fossil fuels, but it presents several problems during thermal conversion processes (combustion, gasification, or pyrolysis) [2–4]. Among other agricultural waste, straw is distinguished by a high content of potassium and silicon (finely distributed in the organic matrix) [5]. It is worth mentioning that the content of potassium and silicon in oat straw is almost identical. Ash from straw combustion contains low-melting potassium-silicates, alkali metals phases like chlorides, sulphates and carbonates which presents serious problems with sintering and the fouling of heat exchangers [6]. Another source of concern for agricultural biomass is the abundant presence of chlorine [7]. Chlorine in biomass occurs mainly in the form of chlorine anion (Cl^-) and is easily soluble in water. Migration behaviours of chlorine during biomass thermal conversion depends on feedstock type. Additionally, chlorine evaporates during the drying and pyrolysis of biomass and forms chloride acid with water vapour [8]. The combustion and pyrolysis of biomass, even at low temperatures (< 600 °C), causes the release of 50% of the initial chlorine content [6, 7]. Chlorine is responsible for the corrosion of devices, where biomass is converted into energy, and for the deactivation of used catalysts. Low-temperature chlorine release from biomass is explained, among other clarifications, by the reaction of KCl with carboxylic groups available in the hemicellulose [6, 8]. The addition of KCl (in the form of an aqueous solution) to the chlorine-free biomass resulted in the release of 30 to 50% of chlorine by

pyrolysis at 400 °C [11]. Furthermore, applying a high heating rate and a small sample size favours chlorine release during a low-temperature pyrolysis [12]. In addition to the heating rate, the sample residence temperature is also important. An increase in the sample residence temperature has a negative effect on chlorine release [13]. Whereas, at a moderate-temperature pyrolysis, oxygen doping into a nitrogen atmosphere promoted HCl release [14]. The type of applied reactor also determines the release of chlorine and its distribution to the pyrolysis products. The hybrid reactor (drop-tube / fixed-bed reactor) allowed for the capture of more chlorine in the char than the fixed-bed reactor [15]. Regardless of the reactor type, Cl-tar dominated the mass balance of chlorine. Furthermore, the co-pyrolysis of inorganic chlorine (polyvinyl chloride) with the biomass favours the enrichment of the oil with chlorine [16].

Another significant factor which determines chlorine release is the content of alkali and alkaline earth metallic species (AAEM), predominantly K, Na, Ca, and Mg in the biomass. Up to 70% of total chlorine can be captured in biomass char at 600 °C because AAEM reacts with HCl [17]. The high efficiency of chlorine captured by char was also confirmed by Knudsen et al. [18]. It was easier to achieve chlorine capture if the biomass contained a lower percentage of chlorine. In the pyrolysis temperature range from 400 to 800 °C, however, 600 °C was the optimal for the maximum captured chlorine in char.

In addition, Wang et al. [19] found that secondary vapour-phase reactions (induced by a higher temperature) led to the redistribution of released chlorine. In light organics, an increase in chlorine content was noted, with a simultaneous reduction of HCl and tar-Cl. Interestingly, the high solubility of HCl in water enables the production of a bio-oil containing low chlorine [20]. When summarizing the literature cited above in Table 1, it

72 was observed that chlorine release was typically reported with long sample residence
73 times in the pyrolysis reactor of 10 to 50 minutes.

74 Table 1. Summary of experimental works on chlorine release during the pyrolysis process

Residence time (min)	Feedstock	Chlorine content in feedstock (%)	Pyrolysis temperature (°C)	Chlorine release	Ref.
10	Corn straw	0.75	300–700	At 500 °C, 75% of the chlorine is released, and at 700 °C, four percent more.	[14]
10	Mallee bark	0.41	400–900	Almost all of the chlorine was released in the fixed-bed reactor. However, in the hybrid reactor (a drop-tube/fixed-bed with continuous feeding) only 50% of chlorine is released at 600 °C.	[15]
15	Wheat straw	0.41	200–1050	60% of chlorine is released at 400 °C. In the 400-700 °C range, there was no significant release of chlorine to the gas phase.	[12]

20	Agricultural waste	0.16–0.26	200–1000	For pyrolysis temperatures higher than 400 °C, 55 to 75% of chlorine was present in the gas phase.	[8]
20	Corn stover	0.69	500–1150	Around 50% of the chlorine was released below 500 °C.	[10]
20	KCl loaded cellulose	0.19–1.64	500, 900	At 500 °C, the chlorine release decreased from 90% to 25% after an increase of KCl (from 0.4 to 3.45%) loaded to the cellulose.	[11]
30	Agricultural biomass	0.06–0.79	200–900	All feedstocks lost between 20-50% of all chlorine at 400 °C. At 400-700 °C, only small changes in the chlorine release occurred.	[9]
30	Wood with PVC	0.01–28.3	750	The release of chlorine to the oil and gas phase was enhanced by	[16]

				increasing the addition of PVC to the wood.	
30-40	Char + 0.16 HCl	3.2	400–800	The char exposed to hydrochloric acid retained nearly 90% of chlorine at 600 °C.	[18]
30	Wood loaded with KCl	0.3	300–500	Use of a two-stage fixed reactor confirmed the redistribution of the chlorine released to light organics and tars as well as 77.5% Cl released into volatiles at 400 °C.	[19]
50	Pine wood doped with 2% KCl	–	300–850	The release of chlorine can be inhibited by reducing the residence time of the biomass particles at temperatures below 500 °C.	[13]

The main goal of this study is to determine the chlorine release under a short residence time (2 minutes) for a sample in the fixed-bed pyrolysis reactor. To the best of the authors' knowledge, such a short sample residence time of 2 min has not yet been analyzed by scientists. Accordingly, a research hypothesis was put forward suggesting

that a short residence time for a sample in the reactor may reduce the release of chlorine to the gas phase. Chlorine release will be investigated at 400, 500 and 600 °C. Four variants of samples will be pyrolysed: i) oat straw (OS), ii) oat straw doped with char, iii) oat straw doped with ammonium chloride, and iv) char doped with ammonium chloride. The addition of chlorine (in the form of ammonium chloride) will enable a better understanding of the influence of inorganic chlorine present in agricultural biomass on its release from both biomass and char. By contrast, the doping of char to biomass will allow for the analysis of the influence of metals on chlorine capture in biochar.

2. Materials and methods

2.1. Feedstocks

Eight types of samples were prepared for pyrolysis. The abbreviated names of the samples used in this work are listed in Table 2. The basic material for this research was oat straw (OS) from a farm located in the Świętokrzyskie Voivodeship (Poland). The oat straw applied for the laboratory pyrolysis experiments was initially dried at room temperature and next ground in the ball mill. The inter-sieve fraction (100–200 μm) was employed for the experiments. A short residence time for the sample in the pyrolysis reactor necessitates the use of small-sized biomass particles. The first variant of the investigations was the pyrolysis of oat straw. The chars, collected at temperatures of 400, 500 and 600 °C (marked as C_400, C_500 and C_600), were used to prepare the next set of samples. Samples for the second variant of the study were obtained by mixing 50% mass of OS and 50% mass of char. These types of samples were prepared to verify the possibility of capturing chlorine from the biomass by char. The addition of char to raw biomass increases the ash content in the sample. The third group of samples was oat straw (96.3% mass) doped with ammonium chloride,

102 NH_4Cl (3.7 mass %). The mass of added NH_4Cl was selected to obtain a 10-fold increase of
103 chlorine content compared to the oat straw. Pure ammonium chloride (white powder) used
104 for the analysis was manufactured by Chempur (Poland).

105 Table 2. List of prepared samples for pyrolysis

Sample No	Name of sample	Feedstock
I	OS	Oat Straw
IIa	OS+C_400	50% OS + 50% Char_400
IIb	OS+C_500	50% OS + 50% Char_500
IIc	OS+C_600	50% OS + 50% Char_600
III	OS+Cl	96.3% OS + 3.7% NH_4Cl
IVa	C_400+Cl	96.3% Char_400 + 3.7% NH_4Cl
IVb	C_500+Cl	96.3% Char_500 + 3.7% NH_4Cl
IVc	C_600+Cl	96.3% Char_600 + 3.7% NH_4Cl

106 The last group of samples were the resulting char from oat straw pyrolysis (first sample)
107 doped with 3.7% mass of ammonium chloride. In the later part of the work, the following
108 names were adopted for the chars: i) a feedstock in samples II and IV are chars, and ii)
109 biochars are solid pyrolysis products for all variants.

110 2.2. Characterization of feedstocks and products

111 Before pyrolysis, OS was milled and dried in a laboratory dryer based on the
112 applicable European Standard ISO 18134-2:2017-03. Other parameters, including the
113 proximate and ultimate analysis of OS were determined on the basis of the following
114 European Standards: ISO 18122:2016-01 – ash content (A), ISO 18123:2016-01 – volatile
115 matter (VM), ISO 16948:2015-07 – carbon (C), hydrogen (H), and nitrogen (N); ISO

16994:2016-10 – sulphur (S), and chlorine (Cl). The extended uncertainty of measurement (k=2) for the determination of the total chlorine in OS was 7%. Additionally, the oxygen content was calculated by difference. The results of the proximate and ultimate analyses of oat straw are shown in Table 3.

Inorganic elements of the studied feedstocks and biochars were detected using the X-ray fluorescence spectroscopy technique (XRF). The measurement was performed by WD-XRF ZSX Primus II Rigaku spectrometer (Rh lamp). Qualitative spectrum analysis was carried out to identify spectral lines. Quantitative analysis was conducted using the SQX Calculation program (Fundamental Parameter Method). The analysis was carried out in the range from fluorine to uranium (F–U), and the content of determined elements was normalized to 100%.

Microstructural and morphological studies were implemented using scanning electron microscopy (SEM), (FEI Inspect S50 device). Studied feedstocks and biochar samples were mounted on metal stubs by double-sided carbon adhesive discs. SEM images were acquired using the secondary electron (SE) detector in the high-vacuum mode. The applied acceleration voltage was 10 keV. Additionally, the microanalysis of the chemical composition was performed using the energy-dispersive X-ray spectroscopy method (EDS) to analyze element distribution.

Table 3. Proximate and ultimate analyses of oat straw

Parameter	Value
Proximate analysis (%, ad [a])	
Moisture (M)	6.03
Volatile Matter (VM)	76.90

Ash (A)	5.64
Fixed Carbon (FC [b])	11.43
Ultimate analysis (%, d [c])	
C	49.94
H	6.77
N	0.69
Cl	0.27
S	0.11
O[d]	36.58

[a]Air-dried basis. [b]FC = 100 – M – VM – A. [c]Dry. [d]By difference.

The chlorine content in the liquid pyrolysis products obtained from the fixed-bed reactor was analyzed by the inductively coupled plasma optical emission spectroscopy (ICP–OES) method. An ICP–OES spectrometer Spectro Arcos SOP (SPECTRO Analytical Instruments, Kleve, Germany) was employed for these investigations.

2.3. Thermal analysis

The preliminary investigations of the pyrolysis process of feedstocks were performed by thermal analysis (TGA). The simultaneous thermal technique was applied to obtain thermogravimetric (TG), differential thermal (DTG) and differential scanning calorimetry data (DSC) (curves). For this purpose, the Mettler Toledo STA apparatus was implemented. The process parameters were as follow: alumina crucible (Al_2O_3), 5 mg of mass sample, atmosphere: nitrogen with flow rate of 50 mL/min, heating rate: 10 °C /min and temperature range: 25–600 °C. The moderate heating rate of 10 °C /min was selected in accordance literature recommendations [21,22].

149 2.4. Pyrolysis at the fixed-bed reactor

150 Laboratory-scale pyrolysis experiments were conducted in an electrically heated
151 fixed-bed reactor, as shown in Fig. 1. Each sample, 1 gram of mass, was pyrolyzed in a
152 nitrogen atmosphere with a volume flow rate of 300 mL/min. The nitrogen flow rate was
153 controlled by digital multiparameter mass flow meter manufactured by AAlborg. For this
154 volumetric nitrogen flow rate, the residence time of the vapours in the reactor was 5 seconds.
155 The short residence time of the pyrolysis vapours in the heating zone promotes oil
156 production.

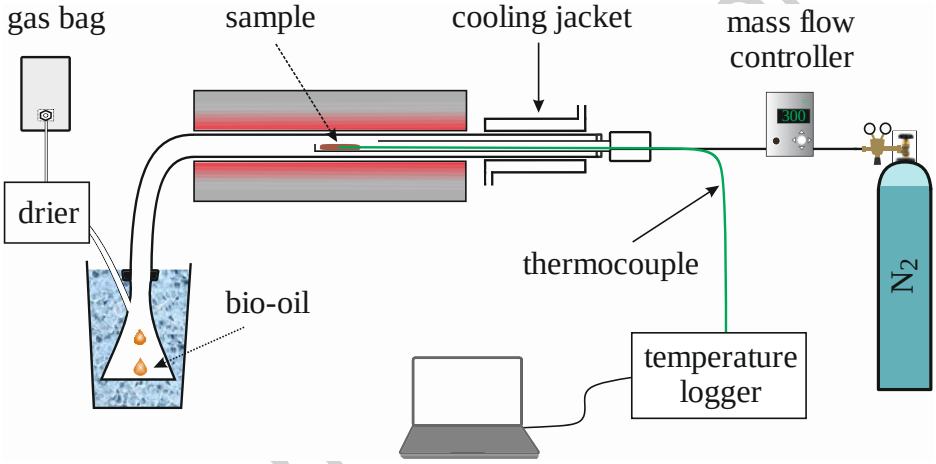

157

158 Fig. 1. Schematic diagram of the laboratory-scale fixed-bed reactor

159 The use of pre-programmed curves shown in Fig. 2, made it possible to carry out the
160 pyrolysis process. In this investigation, the samples were pyrolyzed by heating them to 400,
161 500, 600 °C, with a constant residence time of 2 minutes in the reactor. The temperature of
162 the sample was measured with a K-type thermocouple inside the feedstock. As shown in
163 Fig.2, the pyrolysis process is preceded by a two-minute nitrogen purge of the reactor and
164 the biomass sample is deposited in a water cooling jacket zone. When the sample is placed
165 into the heated reactor, the pyrolysis begins. Pre-programmed curves for heating the samples
166 from approximately 18 °C to 400, 500, 600 °C were characterized by a high heating rate of

274, 343, and 419 °C/min, respectively (average integral calculated as the area under the heating curves related to the heating time). After two minutes, the pyrolyzed sample was moved into a water cooling jacket and then removed and placed under a nitrogen atmosphere for 9 minutes (up to 40 °C).

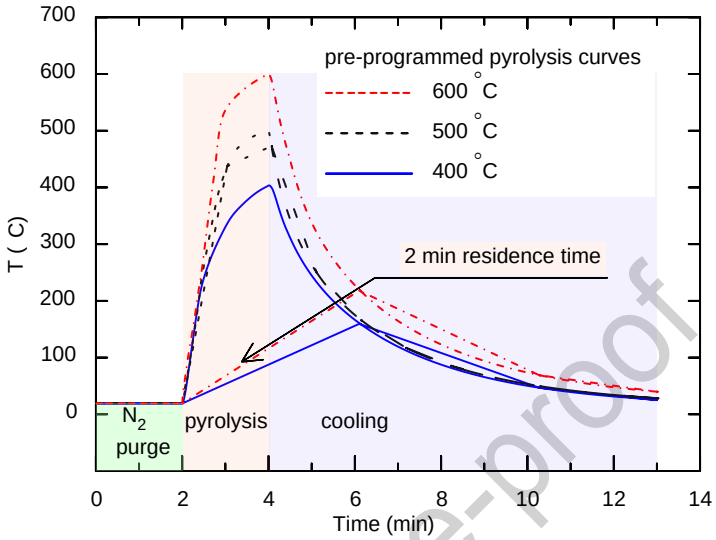

Fig. 2. Pre-programed pyrolysis curves in the fixed-bed reactor

2.5. Pyrolysis at micro scale reactor

Thermal decomposition of OS and OS+Cl samples was performed using Py-GC-MS (Pyroprobe, CDS Analytical: model 5200, connected to a Gas Chromatography Agilent Technologies: model 7890B, equipped with Mass Spectrometry Agilent Technologies: model 5977 A). Prior to the pyrolysis process, the sample weighing 1.0 +/- 0.1 mg, was purged from the air with helium for c.a. 10 min. Pyrolytical investigations were conducted indirect mode at three temperatures, 400, 500, and 600 °C with a heating rate of 100 °C/min and a residence time of 20 s. The experiments were conducted twice for each sample to ensure that the composition of the product could be validated. The Agilent HP-5MS capillary column with dimensions of 60 m × 0.25 mm × 0.25 µm was used for separation. The GC oven temperature programme was as follows: (i) 40 °C with a hold time of 7 min; (ii) heating

ramp from 40 °C to 300 °C at a rate of 4 °C×min^{-1}; (iii) isothermal held at 300 °C for 10 min. The MS spectra were interpreted based on the reference MS library (chemical base G1034C).

3. Results and discussion

3.1. Thermal analysis of feedstocks

The pyrolysis of the studied samples was first investigated using thermal analysis. Figure 3a) shows the thermal analysis of pure NH_4Cl(s), OS, and OS+Cl. The insignificant mass loss of pure ammonium chloride up to the temperature of 198 °C can be attributed to the evaporation of moisture. The thermal decomposition of pure ammonium chloride started at 198 °C, and the decomposition products are NH_3(g) and HCl(g). The maximum sublimation peak on the DTG curve was visible at 258 °C. The TG curve showed the end of sublimation at 329 °C, with a total mass loss of 99.9%. The final sublimation temperature of pure NH_4Cl is consistent with the results of the literature [23,24]. The NH_4Cl sublimation process occurs simultaneously with the decomposition of the OS sample, which consisted of 41.07% cellulose, 24.62% hemicellulose and 5.16% lignin. Zhao et al. [25] reported that maximum decomposition peaks for cellulose, hemicellulose, and lignin were found at 335 °C, 295 °C, and 395 °C, respectively. As the OS sample decomposes, HCl can interact with metal ions in the char matrix.

At 600 °C, approximately 1% more char with OS than OS+Cl remained. On the DTG curves, the maximum peak for OS (-0.82%/°C) falls at a lower temperature of 330 °C than for OS+Cl (-0.66%/°C).

Pyrolysis of OS doped with chars from pyrolysis at 400, 500 and 600 °C are shown in Fig. 3b). The effect of doping OS to chars was an increased content of pyrolysis residues (48.1, 52.5 and 57.3% for OS+C_400, OS+C_500 and OS+C_600 samples, respectively). For all samples, the maximum weight loss was observed at a similar temperature of 325 °C, slightly lower than for pure OS. The DTG peak corresponded to the thermal decomposition of the cellulose [22]. The maximum mass loss during the pyrolysis of the OS+C_500 sample was a surprising result. As shown in the following sections on the basis of XRF and SEM-EDS analyses, sodium, magnesium, and calcium were also present in the samples. These elements have a catalytic effect on the biomass pyrolysis process [26,27]. The local increase in the concentration of these elements could have caused the maximum mass loss for the OS+C_500 sample.

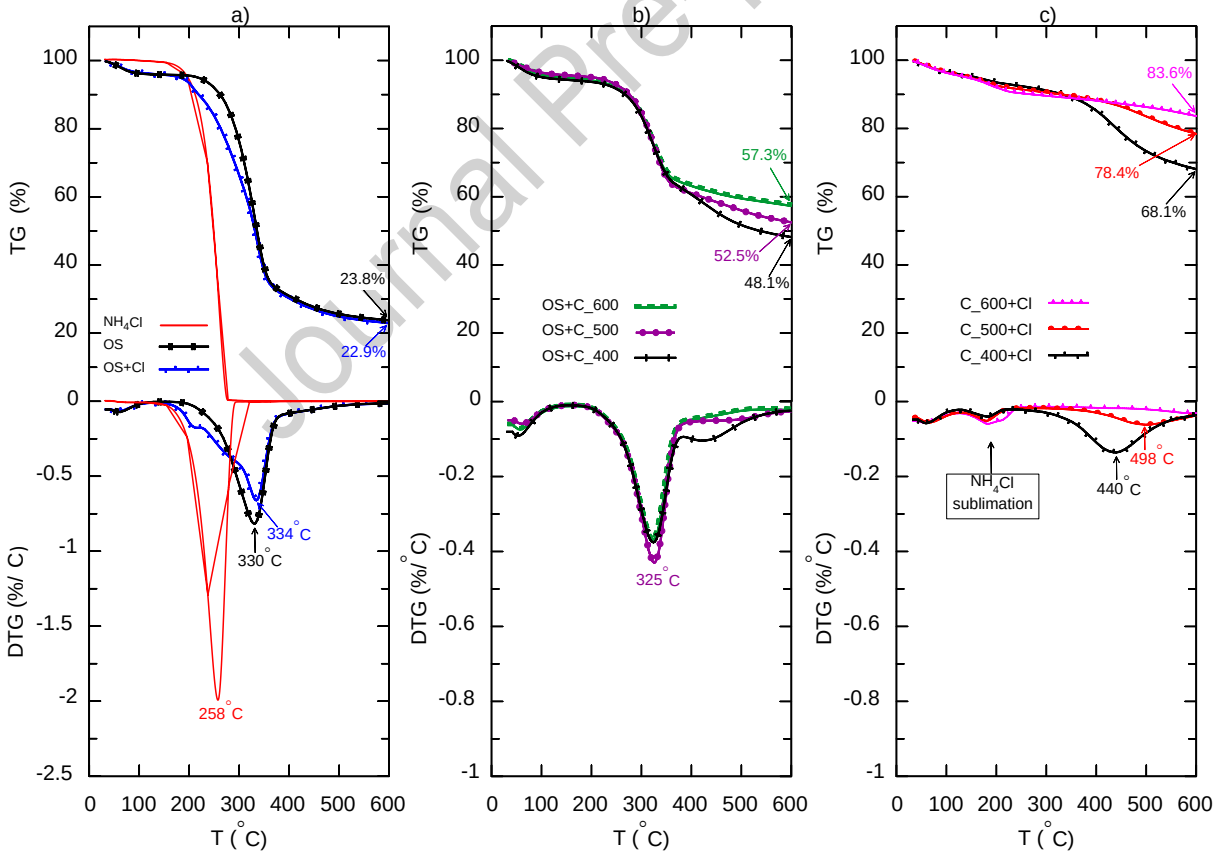

Fig. 3. Thermal analysis of the pyrolysis process under a nitrogen atmosphere for: a) ammonium chloride, oat straw and oat straw doped with NH_4Cl, b) oat straw doped with char from pyrolysis at 400, 500 and 600 °C, and c) char from pyrolysis at 400, 500 and 600 °C doped with NH_4Cl

Fig. 3c) indicates that after the evaporation of moisture for all samples, the sublimation of ammonium chloride occurred. Additionally, the pyrolysis temperature determines the content of volatiles in char. The C_400+Cl sample contained the highest content of volatiles, thus, as a result of its re-pyrolysis, the maximum mass loss was obtained at a temperature of approximately 440 °C.

3.2. Biochar characteristics

Collected biochars (solid pyrolysis product) from experiments performed using a fixed-bed reactor were successively analyzed by ultimate, XRF, and SEM-EDS methods. XRF spectroscopy was sensitive to interactions between elements in the sample and irregular shapes of surfaces. The relative standard error for chlorine measurement in biochars was better than ±6% (typically ±3%).

The results of the ultimate biochar analysis are depicted in Fig. 4a) for carbon, Fig. 4b) for hydrogen and Fig. 4c) for nitrogen. As expected, the carbon content of biochars showed a positive correlation with the pyrolysis temperature. For the OS, according to Table 3, the carbon content was almost 50%. After pyrolysis OS, the carbon content of biochar was 58.4, 59.0, and 61.5% at temperatures of 400, 500 and 600 °C, respectively. Conversely, chars doped with OS slightly improved the carbon content compared to OS biochar. Char doping to OS provided biochar with added value regarding C-conversion efficiency. The addition of ammonium chloride to OS led to similar effects.

Ammonium chloride was a carbonization promotor. Hence, ammonium chloride added to biomass can be an alternative to the popular methods of biomass pre-treatment by washing with acids (hydrochloric acid, acetic acid, sulphuric acid, perchloric acid, nitric acid, etc.) [28,29]. As reported by Pajarito et al., NH_4Cl doped into cellulose as a solid powder was as effective as impregnation with an aqueous solution of NH_4Cl [24].

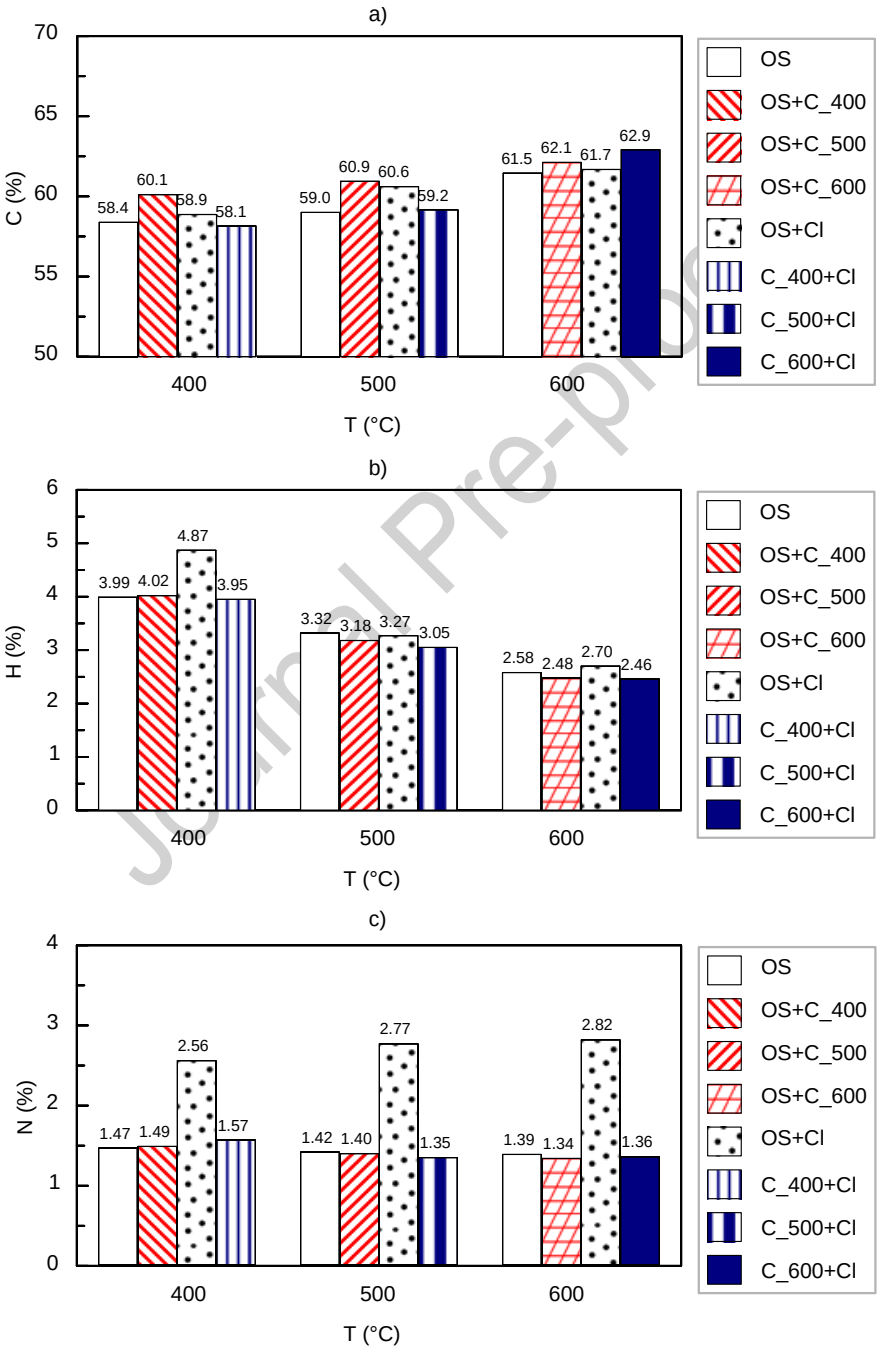

Fig. 4. The content of: a) carbon, b) hydrogen, and c) nitrogen in biochars obtained from pyrolysis

The pyrolysis temperature plays an important role when char doped with ammonium chloride is pyrolyzed. In the case of samples C_400+Cl and C_500+Cl, there was no improvement in carbonization. However, at 600 °C (C_600+Cl sample), the carbon content increased slightly from 61.5% to 62.9%.

Figure 4b) indicates that the short residence time of the sample and the low pyrolysis temperature (400 °C) of OS doped with NH_4Cl favours an increase in the hydrogen content of the sample. The hydrogen content increased in the biochar from 3.99% to 4.87%. The increase of pyrolysis temperature promoted the release of hydrogen into the gas phase for all the prepared samples. A very interesting tendency was observed for the nitrogen content shown in Fig. 4c). Biochar obtained from the OS+Cl pyrolysis was clearly enriched in nitrogen. When the temperature increased, the nitrogen content in biochar also increased. Due to NH_3(g) released during the thermal decomposition of NH_4Cl(s), nitrogen was bound in the biochar. Chen et al. [30] found that biochar could react with NH_3(g) and form numerous N-heterocyclic groups. Generally, to obtain valuable N-containing biochar materials, nitrogen is deliberately fixed in biochar [31]. Biochar's enriched nitrogen values are considered as suitable material for catalysis, energy storage, and CO_2 capture processes [32]. When analyzing the results for samples C_400+Cl, C_500+Cl, and C_600+Cl, it transpired that biochars were not enriched in nitrogen at 500 and 600 °C.

The biochars obtained can be applied as a soil amendment or as a pollutant adsorbent material. The atomic ratios of C:N and H:C in biochars ranged from 25.5 to 51.6 and 0.47 to 1.0, respectively. If the C:N ratio was higher than 20 in biochar or soil, nitrogen was used to support microbial immobilisation in soil [33]. On the other hand, when the H:C values

were in the range of 0.5 to 1.0, the surface active groups played a key role in the adsorption process. As suggested by Wei et al. [34], surface acid groups were positively correlated with the H:C ratio. The growth of such acid groups on the surface of adsorbents promotes the adsorption of metal ions.

Based on the XRF analysis, the contents of chlorine, potassium and silicon in biochars are presented in Fig. 5a-c). When analyzing samples OS+C_400, OS+C_500 and OS+C_600, it can be observed that the addition of the char did not effect chlorine capture in biochar. The most visible changes in chlorine content were in the OS samples doped with NH_4Cl. Increasing the pyrolysis temperature from 400 to 600 °C for the OS+Cl sample significantly improved the chlorine retention in the char, i.e. from 1.43 to 3.27% Cl. However, this is only a preliminary conclusion as it does not take into account the mass of formed biochar. Therefore, a full analysis on the influence of sample type and pyrolysis temperature will be presented taking into account the mass of biochar. The mass of biochar was determined in relation to a 1 gram sample of the feedstock.

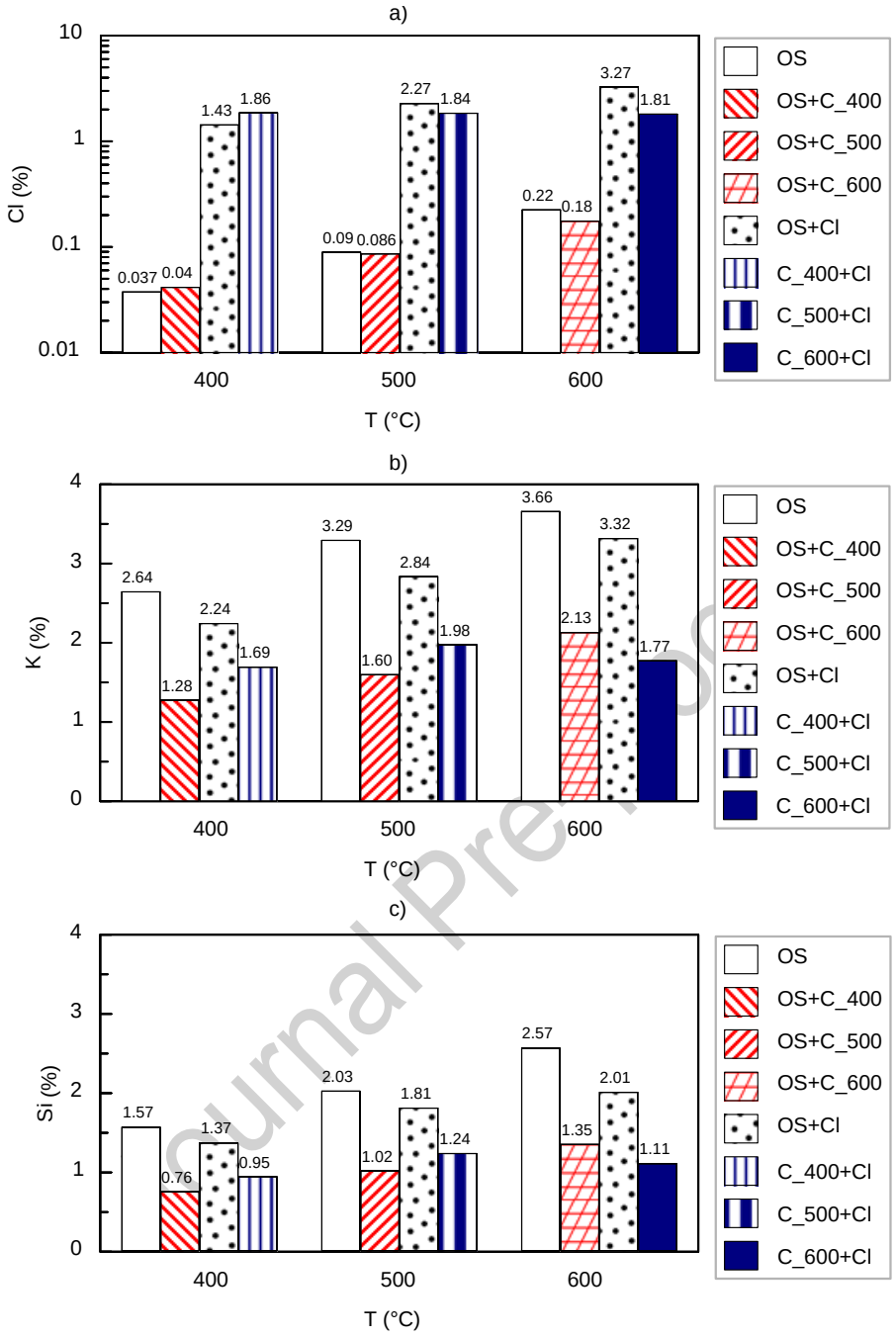

Fig. 5. The content of a) chlorine, b) potassium, and c) silicon in biochars

As shown in Fig. 6, as the pyrolysis temperature increases, the mass of biochar is reduced. Whereas, OS doping with NH_4Cl (OS+Cl) increases the mass of biochar. The previously discussed nitrogen fixed in biochar could be responsible for increasing biochar mass. However, the thermal analysis shown in Fig. 3b) indicates that the mass of OS+Cl

biochar was lower than OS at temperatures of 400, 500 and 600 °C. This result indicates that the heating rate and residence time of the sample had an effect on the mass of biochar. It can be seen in Fig. 6 that samples C_400+Cl, C_500+Cl, and C_600+Cl after pyrolysis at 400, 500, and 600 °C had similar masses of biochar. The concentration of silicon and potassium presented in Fig. 5b) and Fig. 5c) as well as the biochar mass (Fig. 6) were the input data for determining the chlorine release in the next section.

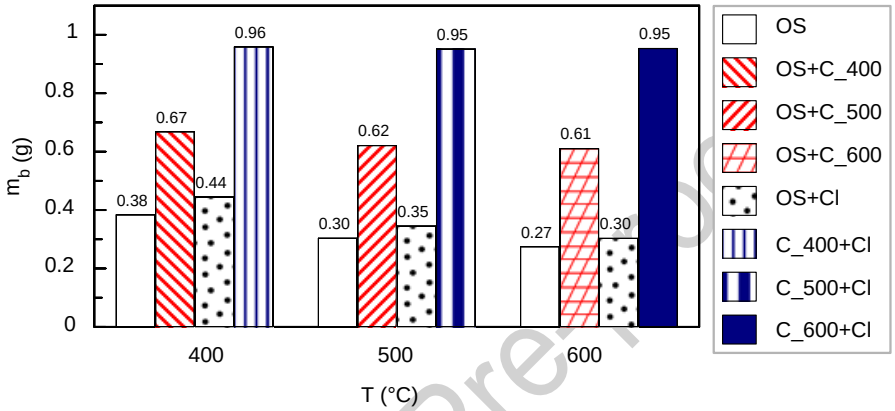

Fig. 6. Mass of biochars at different temperatures

Figures 7a-d) show microphotographs of scanning electron microscopy analysis for biochars obtained under 500 °C. The biochar from OS has a characteristic frayed structure, with irregular shapes. The dark grey surface represents the organic matrix. Two elements of elongated biomass residues stand out in the biochar microphotograph in Fig. 7b), while the white spots in Fig. 7b, Fig. 7c, and Fig. 7d) are separate grains of salt and minerals. The EDS analysis for the micro-area, containing white spots in Fig. 7c) confirmed that it was rich in potassium and chlorine.

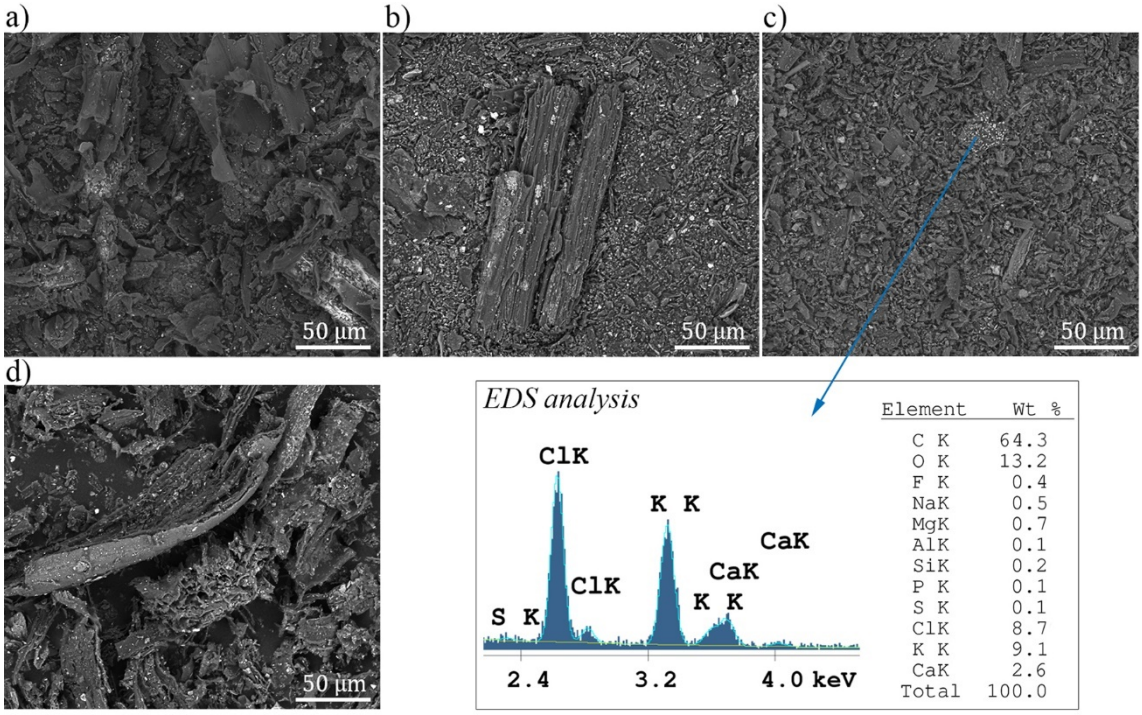

306

307 Fig. 7. SEM images of biochars for: a) OS, b) OS+C_500, c) OS+Cl (with EDS analysis),

308 and d) C_500+Cl

309 A stoichiometric excess of potassium to chlorine indicates the presence of KCl. This may

310 signify that chlorine migrating through the biochar reacts with potassium bound in the

311 biochar matrix to form KCl. Finely ground OS increases the dispersion of potassium in the

312 organic matrix and provides a high reaction surface, which promotes the reactivity of the

313 char in relation to chlorine. The presence of the larger micrometre-range KCl grains,

314 resulting from the reaction of chlorine with potassium contained in the organic matrix, was

315 confirmed by researchers [12,18,35].

316 In Fig. 7d), the biochar obtained from C_500+Cl has cavities with channels which are visible

317 indicating that the structure of the sample contains many free spaces. Moreover, the

318 inorganic chlorine (from NH_4Cl) can lead to the destruction of the carbon structure in biochar

319 and the inhibition of pore formation [36].

320 3.3. Chlorine release

321 Based on a mass balance of chlorine during pyrolysis, the relative release of chlorine
322 to the hot gas phase was calculated by the equation:

323 $$R_{Cl} = \left\{1 - \left(\frac{m_b \cdot \%mass\ Cl_b}{m_f \cdot \%mass\ Cl_f}\right)\right\} \cdot 100\%$$

324 (1)

325 In equation (1), the mass of feedstock (m_f) equals 1 gram, and the mass of biochar (m_b) is
326 consistent with the data in Fig. 6. The mass percentage of chlorine in feedstock samples was
327 determined on the basis of the experimental results and calculations when mixing
328 components. Chlorine content in biochar was taken from Fig. 5a). The verification of the
329 experimental results was carried out using tracer, including two components such as
330 potassium and silicon, according to equation (2)[12]:

331 $$R_{K/Si} = \left\{1 - \left(\frac{\%mass\ K_b/\%mass\ Si_b}{\%mass\ K_f/\%mass\ Si_f}\right)\right\} \cdot 100\%$$

332 (2)

333 The data for equation (2) was the result of XRF analysis in feedstock and biochar. The
334 percentage contents of potassium and chlorine in biochar are consistent with Fig. 5b) and
335 Fig. 5c). The results of the relative chlorine release calculations are depicted in Fig.8a), while
336 the ratio of potassium to silicon (as tracer) is shown in Fig. 8b). Almost 95% by mass of the
337 chlorine contained in OS was released during pyrolysis at the temperature of 400 °C,
338 whereas 50–77.5% has been reported in the literature [5,11,12]. The inter-sieve fraction
339 (100-200 µm) of the OS used for pyrolysis contributed to a high level of chlorine release.
340 OS pyrolysis performed at 600 °C, significantly reduced the R_{Cl} to 77%. This observation
341 confirmed that chlorine released as HCl, and CH_3Cl was captured by char via secondary

reactions [13]. As reported by Knudsen et al. [18], HCl was most effectively captured in the char when the temperature was 600 °C. Inherent metal elements (mainly potassium) at biomass determined the capture of HCl at biochar.

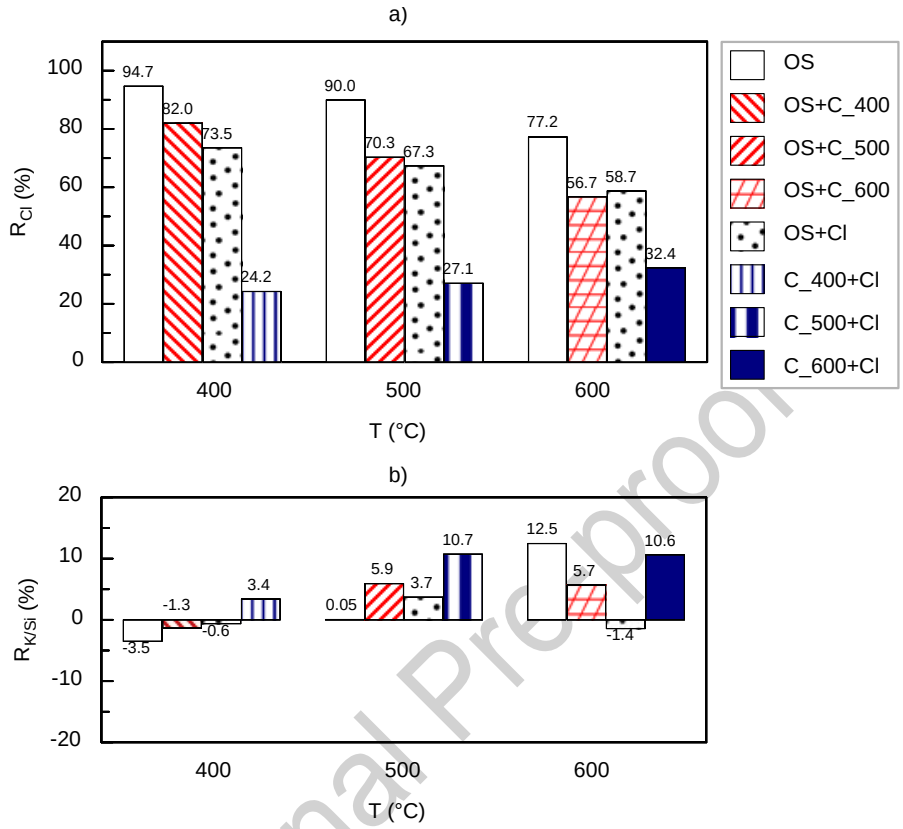

Fig. 8. Relative release of: a) chlorine, and b) potassium/silicon (as tracer), to the hot gas phase

Accordingly, to maximize the chlorine capture in biochar, the pyrolysis process should be conducted at 600 °C. OS doped with chars (OS+C_400, OS+C_500 and OS+C_600) significantly improved the chlorine capture in biochars, because the R_{Cl} dropped from 82% at 400 °C to 56.7% at 600 °C, i.e. by as much as 25.3%. The chlorine capture was improved by doping the OS sample with AAEM-rich char. As a result, AAEM species existing as carbonates or char-bound forms reacted with the chlorine [17,37].

On the contrary, in the OS samples doped with NH_4Cl, chlorine was partially captured in the biochar (at the temperature increased from 400 to 600 °C, the R_{Cl} value was the lower). Although the OS+Cl sample represents a 10-fold higher concentration of Cl compared to pure OS, the R_{Cl} was significantly reduced. The most favourable R_{Cl} value, 24.2%, was obtained for the C_400+Cl sample. Chlorine release was observed, despite increasing temperature pyrolysis of chars doped with NH_4Cl (samples C_400+Cl, C+500+Cl and C_600+Cl). To explain this phenomenon, it is necessary to compare the concentrations of chlorine in the samples before and after pyrolysis (Fig. 5a)). Before pyrolysis, the samples contained 0.04, 0.09 and 0.22% chlorine (in the sample before doping with NH_4Cl), while after pyrolysis in C_400+Cl, C_500+Cl and C_600+Cl chars, the chlorine contents were 1.86, 1.84, 1.81% respectively. Chlorine may have been associated with KCl and char-Cl, and it has reached the saturation state at these temperatures. As a result, the least chlorine amout from the doped NH_4Cl was retained at 600 °C.

The tracer values $R_{K/Si}$ presented in Fig. 8b) for only three samples exceeded 10%, which is considered a good result. Higher values of tracer $R_{K/Si}$ calculated by equation (2) may result from the positive correlation of temperature increase with potassium release [38,39].

3.4. Distribution of chlorine

The concentration of chlorine in liquid pyrolysis products collected during the experiment, which was conducted on a fixed-bed reactor, was determined by the ICP-OES method. The liquid phase was gravimetrically separated into an aqueous phase and oil.

The uncertainty of chlorine measurement was determined according to the recommendations contained in the EURACHEM/CITAC Guide CG4 [40]. The expanded uncertainty at the confidence level of 95% and the expansion factor k=2 for the aqueous

phase was less than 14% and for the oil phase less than 32%. The liquid phases were weighed to determine the yields with the yield of the gas phase (Y_{gas}) estimated as a difference of up to 100%.

$$Y_{gas} = 100\% - Y_b - Y_{oil} - Y_{aq.phase} \quad (3)$$

The biochar yield was calculated using equation (4).

$$Y_b = \frac{m_b}{m_f} \cdot 100\% \quad (4)$$

Based on the chlorine content in pyrolysis products and their yields, the influence of temperature on chlorine distribution is shown in Fig. 9a-f).

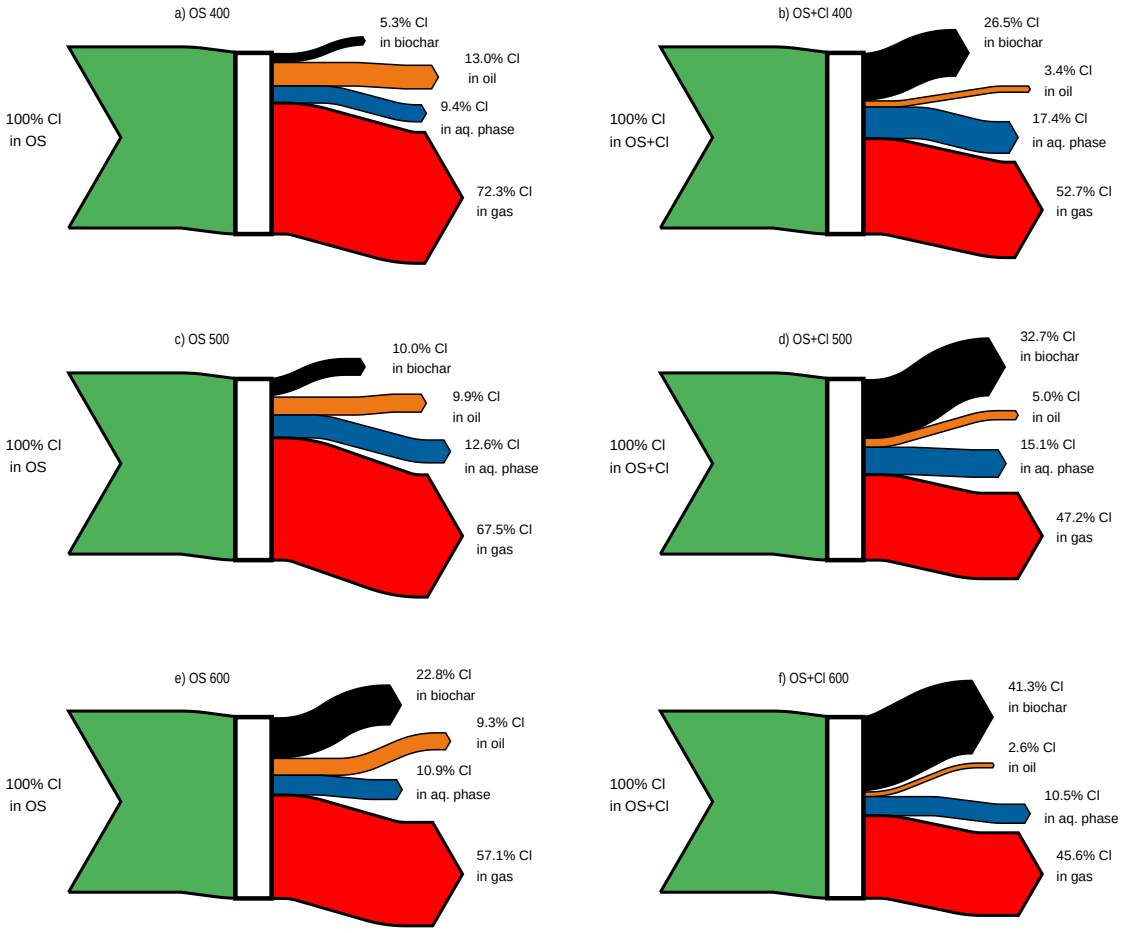

Fig. 9. Distribution of chlorine in pyrolysis products during OS and OS+Cl pyrolysis at a-b) 400, c-d) 500, and e-f) 600 °C

Analyses were performed for two samples OS and OS+Cl. In the case of C_400+Cl, C_500+Cl and C_600+Cl samples, the liquid phase was absent, and for the samples OS+C_400, OS+C_500, and OS+C_600, a very low liquid phase yield was observed. As depicted in Fig. 9a) to Fig. 9f), the reduction of chlorine distribution to the gaseous phase is favoured by higher pyrolysis temperatures. Chlorine was then more easily captured in the biochar, and its percentage increased from 5.3% at 400 °C to 22.8% at 600 °C for the OS sample, while OS doped with NH_4Cl was characterized by a higher percentage of chlorine in the biochars. The percentage of chlorine present in the oil was higher for OS samples (9-13%) compared to OS+Cl (2.6-5.0%). Simultaneously, no correlation was observed between the pyrolysis temperature and the chlorine content in the oil. Only some data from the literature is focussed on the distribution of chlorine to the oil phase [8,41]. As reported by Du et al. [8], the oil contained 10 to 20% of total chlorine. Although, between 14 to 34% of chlorine was for oil in the case of sewage sludge pyrolysis [41]. According to Rahim et al. [15], the dominant percentage of chlorine (~75%) was found in tars from the pyrolysis of bark in a fixed-bed reactor. A high chlorine distribution to tar (up to 64%) was promoted by a low pyrolysis temperature and a high heating rate (600 °C/min) [42].

Chlorine is one of the elements that dissolves rather well in water. For this reason, the distribution of chlorine to the aqueous phase was stronger for the pyrolysis of OS+Cl samples. In this case, the increased chlorine distribution to the gas phase showed a positive correlation with the chlorine distribution to the aqueous phase.

412 3.5. Pyrolysis at micro scale reactor

413 The identification of compounds and the calculation of their relative share was
414 determined by the implementation of the deconvolution algorithm. This was particularly
415 important because of the highly volatile halogenated compounds. Compounds with low
416 molecular weights had a very similar retention time, which, in the case of the integration
417 method, made it impossible to separate them and recognize the compounds.
418 The main compounds detected during pyrolysis OS and OS+Cl are summarized in
419 supplemental materials Table S1. Table 4 depicts a simplified version of Table S1, including
420 groups of compounds identified during Py-GC-MS. The main mechanism of OS and OS+Cl
421 decomposition was based on decarboxylation reactions, as evidenced by the high share of
422 carbon dioxide ranging from 20.92% (for OS+Cl at 600 °C) to 31.38% (for OS at 400 °C).
423 The total area of the carbon dioxide content was favoured by both the increase in pyrolysis
424 temperature and doping with NH_4Cl. The largest group of non-condensing products were
425 various types of oxygen compounds: i) ketones, ii) carboxylic acids, iii) furan derivatives,
426 iv) other oxygenated compounds, and v) phenolic derivatives. Ketones had the largest share
427 (about 19% for all studied temperatures) in the OS pyrolysis product. Doping OS with
428 NH_4Cl reduced the share of ketone compounds for each studied temperature. This doping
429 also had a positive effect on the share of furan derivatives, i.e. dehydration products of
430 polysaccharides made of pentoses such as xylose

431 Table 4. Identified compounds released during the pyrolysis of oat straw and oat straw
432 doped with ammonium chloride by Py–GC–MS cumulative at 400, 500, and 600 °C.

Sample	OS			OS+Cl		
T (°C)	400	500	600	400	500	600

Groups of chemicals / compounds	Area (%)					
Carbon dioxide	31.38	29.28	27.14	25.55	21.43	20.92
Ketones	19.14	18.90	18.91	6.65	10.70	9.31
Carboxylic acids	8.00	7.10	7.02	7.95	7.94	8.64
Furan derivatives	6.71	6.00	2.30	18.50	16.19	13.71
Others oxygenated	6.70	7.76	7.10	2.14	2.35	5.27
Hydrocarbons	4.78	7.13	9.94	3.48	4.53	7.68
Phenol derivatives	3.31	4.74	4.02	2.16	2.22	2.70
N-containing compounds	1.01	2.49	1.39	27.16	27.84	23.86
Cl-containing compounds	0.52	0.36	3.18	5.79	5.51	4.57
% of sum area - identified peaks	81.56	83.78	81.00	99.39	98.71	96.67

and arabinose. The relative share of furan derivatives indicated a negative correlation with an increase in the pyrolysis temperature. The highest shares were at 400 °C with 6.71% and 18.5% for OS and OS+Cl, respectively. Furfural (12.9% – according to Table S1) was the main component of furan derivatives identified during the pyrolysis of the OS+Cl sample conducted at 400 °C. Furfural, produced from biomass, is a valuable feedstock for the chemical industry [43,44]. Table 4 also shows that the higher decomposition temperature of OS and OS+Cl samples promoted the formation of hydrocarbons. The nitrogen contained in ammonium chloride contributed to a strong increase in the content of heterocyclic nitrogen compounds in pyrolysis products. The last group are chlorine-containing compounds. In all temperature conditions, the presence of chloromethane was found for OS and OS+Cl. Non-condensing gases from OS+Cl pyrolysis were richer in chlorine-containing compounds and, in addition to chloromethane, they also contained chloroacetaldehyde.

[1] Conclusion

In this study, the results of experimental investigations of the release of chlorine from: oat straw, oat straw doped with char, oat straw doped with NH_4Cl, and char doped with NH_4Cl during pyrolysis are presented. The novelty of this work was the application of a short residence time (2 minutes) for samples in the pyrolysis reactor. Based on experiments conducted at temperatures of 400, 500 and 600 °C, it was found that:

- Almost 95% of the chlorine was released at 400 °C. The chlorine release was lower when the pyrolysis temperature increased to 600 °C and for the oat straw samples doped with chars.
- Chlorine captured in biochar was confirmed by the presence of KCl.
- NH_4Cl doped with oat straw increased the mass of biochar when the experiment was performed with a short sample residence time. Conversely, the opposite effect was found on the basis of the thermal analysis of a long residence time for the sample.
- The biomass doped with NH_4Cl promoted the fixation of nitrogen in biochar. In addition, biochar yields and carbonization have improved. Another added value of doping oat straw with NH_4Cl was the promotion of furfural production in non-condensable gases.
- A lower percentage distribution of chlorine to oil was noted in the case of the pyrolysis of oat straw doped with NH_4Cl than with oat straw alone.
- The main gaseous Cl-compound detected during Py-GC-MS analysis was chloromethane.

[2] Declaration of competing interest

The authors declare that they have no known competing financial interests or personal relationships that could have appeared to influence the work reported in this paper.

[3] Acknowledgment

This research was funded in whole by the National Science Centre, Poland [grant no. 2020/39/B/ST8/00883]. For the purpose of Open Access, the author has applied a CC-BY public copyright licence to any Author Accepted Manuscript (AAM) version arising from this submission. A shorten version of this research has been presented during the 3rd Sustainable Development of Energy, Water and Environment Systems (SDEWES) Latin American (LA) Conference, São Paulo, Brazil, July 24-28, 2022. The title of the conference paper was “Release of chlorine during oat straw pyrolysis”.

[4] Nomenclature

$\%mass\ Cl_b$	percentage content of chlorine in biochar (%)
$\%mass\ Cl_f$	percentage content of chlorine in feedstock (%)
m_b	mass of biochar (g)
m_f	mass of feedstock (g)
R_{Cl}	relative release of chlorine to gas phase (%)
$R_{K/Si}$	relative release of potassium to gas phase (Si-tracer), (%)
Y_b	yield of biochar (%)
Y_{gas}	yield of gas phase (%)

[5] References

[1] P. Gradziuk, Economic importance and possibilities of using straw for energy

purposes (in polish). The Institute of Soil Science and Plant Cultivation - State Research Institute, IUNG-PIB w Puławach, Poland, 2015. http://www.iung.pulawy.pl.

[2] A. Mlonka-Mędrala, P. Evangelopoulos, M. Sieradzka, M. Zajemska, A. Magdziarz, Pyrolysis of agricultural waste biomass towards production of gas fuel and high-quality char: Experimental and numerical investigations, Fuel. 296 (2021) 120611. https://doi.org/10.1016/j.fuel.2021.120611.

[3] I. Ridjan, B.V. Mathiesen, D. Connolly, N. Duić, The feasibility of synthetic fuels in renewable energy systems, Energy. 57 (2013) 76–84. https://doi.org/10.1016/j.energy.2013.01.046.

[4] T. Sitek, J. Pospíšil, J. Poláčik, M. Špiláček, P. Varbanov, Fine combustion particles released during combustion of unit mass of beechwood, Renew. Energy. 140 (2019) 390–396. https://doi.org/10.1016/j.renene.2019.03.089.

[5] M. Zevenhoven, P. Yrjas, B.J. Skrifvars, M. Hupa, Characterization of ash-forming matter in various solid fuels by selective leaching and its implications for fluidized-bed combustion, Energy and Fuels. 26 (2012) 6366–6386. https://doi.org/10.1021/ef300621j.

[6] Y. Niu, H. Tan, S. Hui, Ash-related issues during biomass combustion: Alkali-induced slagging, silicate melt-induced slagging (ash fusion), agglomeration, corrosion, ash utilization, and related countermeasures, Prog. Energy Combust. Sci. 52 (2016) 1–61. https://doi.org/10.1016/j.pecs.2015.09.003.

[7] F. Li, B. Yu, J. Li, Z. Wang, M. Guo, H. Fan, T. Wang, Y. Fang, Exploration of potassium migration behavior in straw ashes under reducing atmosphere and its modification by additives, Renew. Energy. 145 (2020) 2286–2295.

https://doi.org/10.1016/j.renene.2019.07.141.

[8] S. Du, X. Wang, J. Shao, H. Yang, G. Xu, H. Chen, Releasing behavior of chlorine and fluorine during agricultural waste pyrolysis, Energy. 74 (2014) 295–300. https://doi.org/10.1016/j.energy.2014.01.012.

[9] B. Strömberg, E. Björkman, Release of chlorine from biomass and model compounds at pyrolysis and gasification conditions, Energy and Fuels. 11 (1997) 1026–1032. https://doi.org/10.1021/ef970031o.

[10] J.M. Johansen, J.G. Jakobsen, F.J. Frandsen, P. Glarborg, Release of K, Cl, and S during pyrolysis and combustion of high-chlorine biomass, Energy and Fuels. 25 (2011) 4961–4971. https://doi.org/10.1021/ef201098n.

[11] H. Zhao, Q. Song, Q. Yao, Release and transformation of K and Cl during the pyrolysis of KCl-loaded cellulose, Fuel. 226 (2018) 583–590. https://doi.org/10.1016/j.fuel.2018.04.068.

[12] P.A. Jensen, F.J. Frandsen, K. Dam-Johansen, B. Sander, Experimental investigation of the transformation and release to gas phase of potassium and chlorine during straw pyrolysis, Energy and Fuels. 14 (2000) 1280–1285.

[13] Y. Wang, H. Wu, Z. Sárossy, C. Dong, P. Glarborg, Release and transformation of chlorine and potassium during pyrolysis of KCl doped biomass, Fuel. 197 (2017) 422–432. https://doi.org/10.1016/j.fuel.2017.02.046.

[14] J. Cheng, M. Xie, L. Xu, L. Zhang, X. Ren, Chlorine release from co-pyrolysis of corn straw and lignite in nitrogen and oxidative pyrolysis, Energies. 14 (2021) 8227. https://doi.org/10.3390/en14248227.

[15] M.U. Rahim, X. Gao, M. Garcia-Perez, Y. Li, H. Wu, Release of chlorine during mallee bark pyrolysis, Energy and Fuels. 27 (2013) 310–317.

https://doi.org/10.1021/ef3018157.

[16] A. Ephraim, D. Pham Minh, D. Lebonnois, C. Peregrina, P. Sharrock, A. Nzihou, Co-pyrolysis of wood and plastics: Influence of plastic type and content on product yield, gas composition and quality, Fuel. 231 (2018) 110–117. https://doi.org/10.1016/j.fuel.2018.04.140.

[17] H. Zhao, Q. Song, Q. Yao, HCl Capture by Rice Straw Char and Its Influence on the Transformation of Alkali and Alkaline Earth Metallic Species during Pyrolysis, Energy and Fuels. 30 (2016) 5854–5861. https://doi.org/10.1021/acs.energyfuels.6b00984.

[18] J.N. Knudsen, P.A. Jensen, W. Lin, K. Dam-Johansen, Secondary capture of chlorine and sulfur during thermal conversion of biomass, Energy and Fuels. 19 (2005) 606–617. https://doi.org/10.1021/ef049874n.

[19] B. Wang, J. Huang, X. Gao, Y. Qiao, Effects of Secondary Vapor-Phase Reactions on the Distribution of Chlorine Released from the Pyrolysis of KCl-Loaded Wood, Energy and Fuels. 34 (2020) 11717–11721. https://doi.org/10.1021/acs.energyfuels.0c02320.

[20] W.M. Koo, S.H. Jung, J.S. Kim, Production of bio-oil with low contents of copper and chlorine by fast pyrolysis of alkaline copper quaternary-treated wood in a fluidized bed reactor, Energy. 68 (2014) 555–561. https://doi.org/10.1016/j.energy.2014.02.020.

[21] H. Stančin, M. Šafář, J. Růžičková, H. Mikulčić, H. Raclavská, X. Wang, N. Duić, Influence of plastic content on synergistic effect and bio-oil quality from the co-pyrolysis of waste rigid polyurethane foam and sawdust mixture, Renew. Energy. 196 (2022) 1218–1228. https://doi.org/10.1016/j.renene.2022.07.047.

561 [22] S. Wang, Y. Wen, H. Hammarström, P.G. Jönsson, W. Yang, Pyrolysis behaviour,
562 kinetics and thermodynamic data of hydrothermal carbonization–Treated pulp and
563 paper mill sludge, Renew. Energy. 177 (2021) 1282–1292.
564 https://doi.org/10.1016/j.renene.2021.06.027.
565 [23] H.G. Stewart, T.D. Humphries, D.A. Sheppard, M.S. Tortoza, M.V. Sofianos, S.
566 Liu, C.E. Buckley, Ammonium chloride-metal hydride based reaction cycle for
567 vehicular applications, J. Mater. Chem. A. 7 (2019) 5031–5042.
568 https://doi.org/10.1039/c9ta00192a.
569 [24] B.B. Pajarito, C. Llorens, T. Tsuzuki, Effects of ammonium chloride on the yield
570 of carbon nanofiber aerogels derived from cellulose nanofibrils, Cellulose. 26
571 (2019) 7727–7740. https://doi.org/10.1007/s10570-019-02645-0.
572 [25] C. Zhao, E. Jiang, A. Chen, Volatile production from pyrolysis of cellulose,
573 hemicellulose and lignin, J. Energy Inst. 90 (2017) 902–913.
574 https://doi.org/10.1016/j.joei.2016.08.004.
575 [26] A. Alcazar-Ruiz, M.L. Ortiz, L. Sanchez-Silva, F. Dorado, Catalytic effect of alkali
576 and alkaline earth metals on fast pyrolysis pre-treatment of agricultural waste,
577 Biofuels, Bioprod. Biorefining. 15 (2021) 1473–1484.
578 https://doi.org/10.1002/bbb.2253.
579 [27] G. Yildiz, F. Ronsse, R. Venderbosch, R. van Duren, S.R.A. Kersten, W. Prins,
580 Effect of biomass ash in catalytic fast pyrolysis of pine wood, Appl. Catal. B
581 Environ. 168–169 (2015) 203–211. https://doi.org/10.1016/j.apcatb.2014.12.044.
582 [28] A. Singhal, M. Goossens, J. Konttinen, T. Joronen, Effect of basic washing
583 parameters on the chemical composition of empty fruit bunches during washing
584 pretreatment: A detailed experimental, pilot, and kinetic study, Bioresour. Technol.

340 (2021) 125734. https://doi.org/10.1016/j.biortech.2021.125734.

[29] S. Hosseinpour, M.A. Babatabar, M. V. Mousavi, A. Tavasoli, Production of high-quality bio-product by pyrolysis of acid/metal modified chickpea husk, Int. J. Energy Res. 46 (2022) 20228–20248. https://doi.org/10.1002/er.8480.

[30] W. Chen, H. Yang, Y. Chen, K. Li, M. Xia, H. Chen, Influence of Biochar Addition on Nitrogen Transformation during Copyrolysis of Algae and Lignocellulosic Biomass, Environ. Sci. Technol. 52 (2018) 9414–9521. https://doi.org/10.1021/acs.est.8b02485.

[31] X. Zhang, S. Zhang, H. Yang, J. Shao, Y. Chen, X. Liao, X. Wang, H. Chen, Generalized two-dimensional correlation infrared spectroscopy to reveal mechanisms of CO2 capture in nitrogen enriched biochar, Proc. Combust. Inst. 36 (2017) 3933–3940. https://doi.org/10.1016/j.proci.2016.06.062.

[32] W. Chen, Y. Chen, H. Yang, M. Xia, K. Li, X. Chen, H. Chen, Co-pyrolysis of lignocellulosic biomass and microalgae: Products characteristics and interaction effect, Bioresour. Technol. 245 (2017) 860–868. https://doi.org/10.1016/j.biortech.2017.09.022.

[33] T.T.N. Nguyen, C.Y. Xu, I. Tahmasbian, R. Che, Z. Xu, X. Zhou, H.M. Wallace, S.H. Bai, Effects of biochar on soil available inorganic nitrogen: A review and meta-analysis, Geoderma. 288 (2017) 79–96. https://doi.org/10.1016/j.geoderma.2016.11.004.

[34] L. Wei, Y. Huang, L. Huang, Y. Li, Q. Huang, G. Xu, K. Müller, H. Wang, Y.S. Ok, Z. Liu, The ratio of H/C is a useful parameter to predict adsorption of the herbicide metolachlor to biochars, Environ. Res. 184 (2020). https://doi.org/10.1016/j.envres.2020.109324.

609 [35] W. Kaniowski, J. Taler, X. Wang, I. Kalemba-Rec, M. Gajek, A. Mlonka-Mędrala,
610 D. Nowak-Woźny, A. Magdziarz, Investigation of biomass, RDF and coal ash-
611 related problems: Impact on metallic heat exchanger surfaces of boilers, Fuel. 326
612 (2022). https://doi.org/10.1016/j.fuel.2022.125122.
613 [36] B. Hu, Q. Huang, A.C.T. Bourtsalas, M. Ali, Y. Chi, J. Yan, Effect of Chlorine on
614 the Structure and Reactivity of Char Derived from Solid Waste, Energy and Fuels.
615 31 (2017) 7606–7616. https://doi.org/10.1021/acs.energyfuels.7b01042.
616 [37] J.N. Knudsen, P.A. Jensen, K. Dam-Johansen, Transformation and release to the
617 gas phase of Cl, K, and S during combustion of annual biomass, Energy and Fuels.
618 18 (2004) 1385–1399. https://doi.org/10.1021/ef049944q.
619 [38] Z. Tan, L. Zhang, Q. Huang, A comparison of CO2, N2, and Ar to maximize plant
620 nutrient retention in biochar, Clean Technol. Environ. Policy. 20 (2018) 421–426.
621 https://doi.org/10.1007/s10098-017-1472-4.
622 [39] C. Chen, Z. Luo, C. Yu, T. Wang, H. Zhang, Transformation behavior of potassium
623 during pyrolysis of biomass, RSC Adv. 7 (2017) 31319–31326.
624 https://doi.org/10.1039/c7ra05162j.
625 [40] S.L.R. Ellison, A. Williams, eds., Quantifying Uncertainty in Analytical
626 Measurement, Third Edit, Eurachem/CITAC, Teddington, UK, 2012.
627 https://doi.org/10.25607/OBP-952.
628 [41] Y. Liu, C. Ran, A.R. Siddiqui, P. Chtaeva, A.A. Siyal, Y. Song, J. Dai, Z. Deng, J.
629 Fu, W. Ao, Z. Jiang, T. Zhang, Pyrolysis of sewage sludge in a benchtop fluidized
630 bed reactor: Characteristics of condensates and non-condensable gases, Renew.
631 Energy. 160 (2020) 707–720. https://doi.org/10.1016/j.renene.2020.06.137.
632 [42] Y. Ren, C. Cao, H. Hu, S. Lei, X. Yuan, X. Li, H. Yao, Transformation behavior

633 and fate of chlorine in polychloroprene (PCP) during its pyrolysis, Fuel. 317 (2022)
634 123573. https://doi.org/10.1016/j.fuel.2022.123573.
635 [43] Y. Luo, Z. Li, X. Li, X. Liu, J. Fan, J.H. Clark, C. Hu, The production of furfural
636 directly from hemicellulose in lignocellulosic biomass: A review, Catal. Today.
637 319 (2019) 14–24. https://doi.org/10.1016/j.cattod.2018.06.042.
638 [44] S. Sobek, K. Zeng, S. Werle, R. Junga, M. Sajdak, Brewer's spent grain pyrolysis
639 kinetics and evolved gas analysis for the sustainable phenolic compounds and fatty
640 acids recovery potential, Renew. Energy. 199 (2022) 157–168.
641 https://doi.org/10.1016/j.renene.2022.08.114.
642

643 Credit Author Statement

644

645 **Wojciech Jerzak:** Conceptualization, Methodology, Investigation, Writing - Original

646 Draft, Review & Editing, Resources, Visualization; **Mariusz Wądrzyk:** Formal analysis,

647 Investigation, Writing - original draft; **Izabela Kalemba-Rec:** Data curation,

648 Investigation, Writing - original draft; **Artur Bieniek:** Data curation, Investigation,

649 Writing - original draft; **Aneta Magdziarz:** Writing - Review & Editing, Supervision,

650 Project administration, Funding acquisition.